Transmembrane helix 6b links proton and metal release pathways and drives conformational change in an Nramp-family transition metal transporter

Received for publication, October 3, 2019, and in revised form, December 10, 2019 Published, Papers in Press, December 27, 2019, DOI 10.1074/jbc.RA119.011336

Aaron T. Bozzi[1], **Anne L. McCabe**[2], **Benjamin C. Barnett**[3], **and Rachelle Gaudet**[4]

From the Department of Molecular and Cellular Biology, Harvard University, Cambridge, Massachusetts 02138

Edited by Karen G. Fleming

The natural resistance-associated macrophage protein (Nramp) family encompasses transition metal and proton cotransporters that are present in many organisms from bacteria to humans. Recent structures of *Deinococcus radiodurans* Nramp (DraNramp) in multiple conformations revealed the intramolecular rearrangements required for alternating access of the metal-binding site to the external or cytosolic environment. Here, using recombinant proteins and metal transport and cysteine accessibility assays, we demonstrate that two parallel cytoplasm-accessible networks of conserved hydrophilic residues in DraNramp, one lining the wide intracellular vestibule for metal release and the other forming a narrow proton transport pathway, are essential for metal transport. We further show that mutagenic or posttranslational modifications of transmembrane helix (TM) 6b, which structurally links these two pathways, impede normal conformational cycling and metal transport. TM6b contains two highly conserved histidines, His^{232} and His^{237}. We found that different mutagenic perturbations of His^{232}, just below the metal-binding site along the proton exit route, differentially affect DraNramp's conformational state, suggesting that His^{232} serves as a pivot point for conformational changes. In contrast, any replacement of His^{237}, lining the metal exit route, locked the transporter in a transport-inactive outward-closed state. We conclude that these two histidines, and TM6b more broadly, help trigger the bulk rearrangement of DraNramp to the inward-open state upon metal binding and facilitate return of the empty transporter to an outward-open state upon metal release.

Approximately one-third of all proteins require specific metal ion cofactors (1) that bind in dedicated sites to stabilize tertiary structures, impart catalytic properties to enzymes, increase protein affinity for other ligands, and enable electron transfer. To maintain metal homeostasis, organisms must acquire metal ions in sufficient quantity from their environment, traffic them to their proper destination, and safely store or excrete any excess to avoid toxicity (2, 3). Natural resistance-associated macrophage proteins (Nramps)[5] are transporters that harness the electrochemical energy of proton gradients and the membrane potential to power the uptake of divalent transition metals (4–8). Nramp homologs scavenge manganese in bacteria (9) and acquire and traffic manganese and iron in plants (10) and fungi (11). In mammals, one homolog, Nramp2 (also known as divalent metal transport 1 (DMT1)) facilitates dietary iron uptake in the duodenum (12, 13) and erythroblast iron loading in the bone marrow (14, 15), whereas the eponymous homolog Nramp1 helps phagocytes kill engulfed pathogens by extracting essential metals from phagosomes (16–18).

We developed the *Deinococcus radiodurans* Nramp (DraNramp) homolog as a model system to understand the general mechanism of this family of transporters (4, 19–21). DraNramp is the sole high-affinity Mn^{2+} uptake system (22, 23) for a species that maintains an exceptionally high intracellular Mn^{2+} concentration as a resistance mechanism to radiation damage (24); thus, it may be a particularly robust transporter, given the likely demand for high expression and activity *in vivo*. Crystal structures of DraNramp in outward-open, inward-occluded, and inward-open states revealed a LeuT-fold, common among secondary transporters (25), and conformations consistent with an alternating access model (20, 21). Transmembrane helices (TMs) 1, 4, 5, 6, and 10 undergo the greatest displacement relative to each other and to the remaining six TMs, which function as a "scaffold" to support those movements (21, 26). Furthermore, although metal transport requires bulk conformational change between outward- and inward-open states, proton uniport occurs through the outward-open but not inward-open state (21). Thus, metal ions and protons transit the external aqueous vestibule to reach their conserved binding site (Asp^{56} for protons and Asp^{56} along with Asn^{59}, Met^{230}, and the Ala^{53} and Ala^{227} carbonyls for metals (21, 27)) in the center of the protein but take separate pathways from there to reach the cytoplasm (21).

This work was funded in part by National Institutes of Health Grant R01GM120996 (to R. G.). The authors declare that they have no conflicts of interest with the contents of this article. The content is solely the responsibility of the authors and does not necessarily represent the official views of the National Institutes of Health.

This article contains Figs. S1–S3.

[1] Present address: Alexion Pharmaceuticals, 100 College St., New Haven, CT 06510.

[2] Present address: Dept. of Molecular Biology and Microbiology, Tufts University School of Medicine, 885 Washington St., Boston, MA 02111.

[3] Present address: UNC School of Medicine, 321 S. Columbia St., Chapel Hill, NC 27599.

[4] To whom correspondence should be addressed: Dept. of Molecular and Cellular Biology, Harvard University, 52 Oxford St., Cambridge, MA 02138. Tel.: 617-495-5616; E-mail: gaudet@mcb.harvard.edu.

[5] The abbreviations used are: Nramp, natural resistance-associated macrophage protein; Dra, *Deinococcus radiodurans*; NEM, *N*-ethylmaleimide; TM, transmembrane helix.

Here we first identify separate clusters of conserved hydrophilic residues that line each of these pathways. Point mutations to alanine at most of these positions impair DraNramp Mn^{2+} and Co^{2+} transport. Both of these hydrophilic networks are important for metal transport, which helps explain how naturally occurring mutations in mammalian DMT1 abrogate the transporter's function to cause anemia.

The highly conserved TM6b forms the clearest structural connection between these two networks. In the second half of the paper, we use chemical modifications of a panel of single-cysteine mutants that span TM6 to show that adding steric bulk at many positions along the helix eliminates metal transport, likely by blocking essential conformational rearrangements. Furthermore, alanine replacement of several conserved hydrophilic and hydrophobic TM6b residues impedes DraNramp from sampling the outward-open state, as assessed using a single-cysteine reporter. Last, using a range of amino acid replacements for two highly conserved histidines, we show that any perturbation of His^{237} locks the transporter in a transport-inactive, outward-closed state, whereas substitutions of His^{232} have a range of effects on DraNramp's transport activity and conformational preferences that suggest that His^{232} may be a pivot point for conformational change.

From all our results, we conclude that TM6b, and its two histidines in particular, plays a critical role in the conformational change process required for metal transport. As the structural connection between the two hydrophilic intracellular substrate release pathways, TM6b may sense metal binding and/or the ensuant proton transfer to help convert local changes into the bulk conformational rearrangement required to complete the metal transport process.

Results

Conserved hydrophilic residues cluster in two networks on DraNramp's cytoplasmic side

DraNramp consists of 11 TMs, the first 10 of which adopt the canonical LeuT inverted repeat of two pseudosymmetric five-TM units. We used our previously published alignment of 6878 Nramp sequences that include the canonical DPGN and MPH motifs (21) and determined the positions at which hydrophilic residues predominate (defined as Ser + Thr + Tyr + Asn + Gln +Asp + Glu + His + Lys + Arg > 80%) (Fig. S1). We then mapped these positions onto our outward-open and inward-open DraNramp structures (Fig. 1). There is a notable paucity of conserved hydrophilic positions in the external half of the transporter, with only a few hydrophilic residues lining the wide aqueous vestibule that provides access to the metal-binding site (Fig. 1). Thus, predominantly hydrophobic packing between TMs 1b, 3, 6a, 8, and 10 seals this external vestibule in the inward-open state (20, 21). In contrast, a number of hydrophilic positions flank the conserved metal-binding site in the middle of the membrane, and the cytoplasmic half of the protein is rich in hydrophilic residues. The positions in the protein's lower half form two extended polar networks. One, between TMs 1a, 2, 5, 6a, and 7, lines the wide intracellular vestibule that serves as the metal release pathway in the inward-open state (Fig. 1) (20). The second, between TMs 3, 4, 8, and 9,

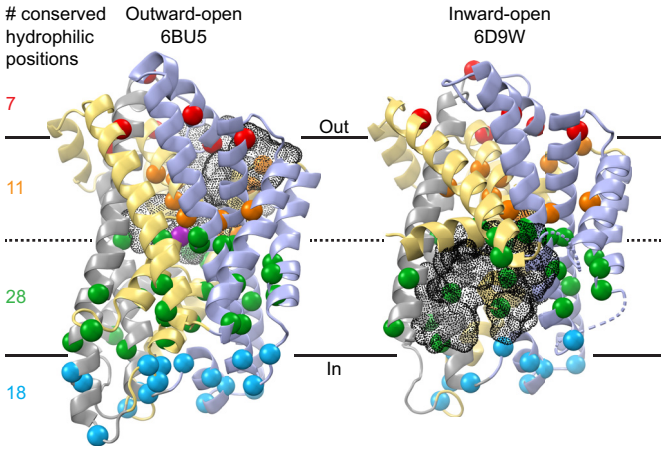

Figure 1. Conserved hydrophilic positions cluster on the intracellular side of DraNramp. Cα positions at which Ser + Thr + Tyr + Asn + Gln +Asp + Glu + His + Lys + Arg > 80% from an alignment of 6878 Nramps are shown as *colored spheres* on the outward-open Mn^{2+}-bound (PDB code 6BU5) and inward-open apo (PDB code 6D9W) structures of DraNramp (21). TMs 1, 5, 6, and 10 are *gold*, TMs 2, 7, and 11 are *gray*, and TMs 3, 4, 8, and 9 are *blue*. The Mn^{2+} substrate is *magenta* in the outward-open structure. The external and internal vestibules that enable metal entry and release are shown as *black mesh*. A sequence logo based on the alignment is shown in Fig. S1.

forms the narrow pathway that provides a route for proton uniport in the outward-open state (21) as well as metal-stimulated proton transport (4). These two networks meet at the conserved proton/metal-binding site (6, 21, 27), where they provide parallel exit pathways that facilitate cotransport of two like charges (21).

To assess the importance of these residues to the general metal transport mechanism, we generated a panel of DraNramp point mutants that we expressed in *Escherichia coli* (Figs. S1 and S2). We then measured relative rates of *in vivo* Co^{2+} transport (WT $K_m \approx 1$ mM (4)) via our established colorimetric assay (19) and Mn^{2+} transport (WT $K_m \approx 3$ μM (4, 21)) with a new assay in which metal uptake is monitored through the increase in fluorescence of intracellular GCaMP6f (Fig. S3). We discuss the results of these experiments below in the context of our recent high-resolution crystal structures of outward-open and inward-occluded DraNramp (21) as we explore the roles of the two polar networks in DraNramp function.

Mutations to the nonhelical binding-site region impair metal transport

Consistent with other LeuT-fold transporters (28, 29), DraNramp uses nonhelical regions in the middle of TM1 and TM6 to bind substrates (21, 27). In the outward-open state, Asp^{56}, Asn^{59}, and the Ala^{53} backbone carbonyl from TM1 and Met^{230} from TM6 coordinate Mn^{2+} (21). In the inward-open state, Asp^{56}, Asn^{59}, and Met^{230} still coordinate Mn^{2+}, but the increasing helicity of TM6a enables the Ala^{227} backbone carbonyl to replace the Ala^{53} backbone carbonyl in the Mn^{2+} coordination sphere in a structure of the related *Staphylococcus capitis* Nramp (27). In addition, Gln^{378} (86% conserved in our alignment, another 11% as N) from TM10 may also directly or indirectly stabilize Mn^{2+} in an occluded conformation (19, 21, 30). To stabilize the extended unwinding of TM6a in the outward-open state, TM6's Thr^{228} (80% conserved) and TM11's Asn^{426} (99% conserved) donate hydrogen bonds to the unsatis-

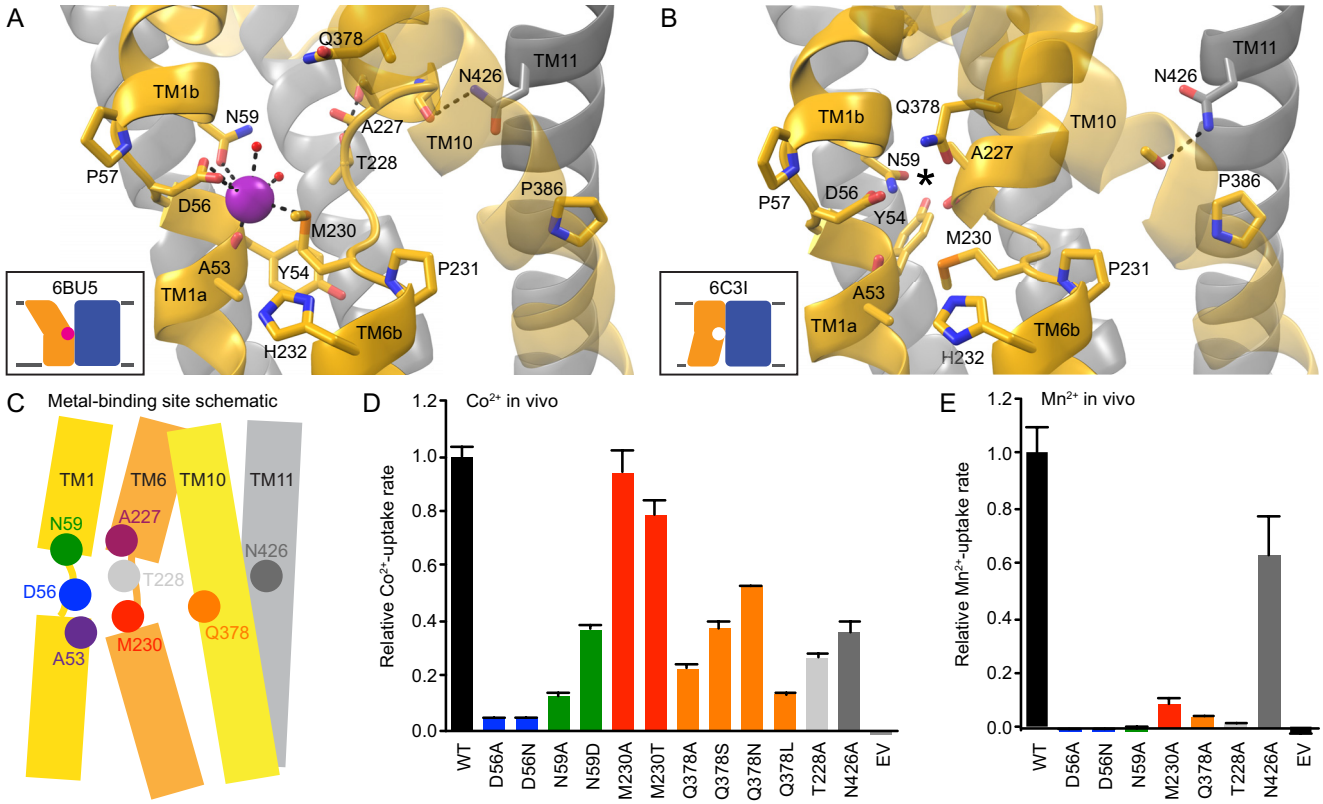

Figure 2. Unwound regions form a conserved metal binding site. *A* and *B*, side view of the metal-binding site region, with the intracellular face of the protein pointing down. For clarity, only TMs 1, 2, 6, 7, 10, and 11 are shown. *A*, conserved Asp[56], Asn[59], and Met[230] side chains along with the Ala[53] carbonyl and two ordered waters coordinate the Mn^{2+} substrate in the outward-open state (PDB code 6BU5). Extended TM6 unwinding is facilitated by the Thr[228] and Asn[426] side chains donating hydrogen bonds to TM6 backbone carbonyls. *B*, in the inward-occluded apo state (PDB code 6C3I), the toppling of TM10 above the conserved Pro[386] enables Gln[378] to approach the other metal-binding side chains, whereas helical extension of TM6a brings the Ala[227] carbonyl into the metal-binding site (an *asterisk* indicates the expected location for a bound metal ion in this and subsequent figures). *C*, schematic of important residues in the unwound metal-binding site. *D* and *E*, most mutations to conserved binding-site residues impaired relative *in vivo* Co^{2+} (*D*) and Mn^{2+} (*E*) uptake rates. *EV*, empty vector (no DraNramp) control. Data are averages ± S.E. ($n \geq 4$ for Co^{2+} and $n \geq 6$ for Mn^{2+}).

fied backbone carbonyls of Ile[224] and Gly[226], respectively (Fig. 2*A*). In contrast, in the inward-occluded state, both side chains reorient to allow TM6a to extend by two residues, with Asn[426] now donating a hydrogen bond to the carbonyl of Cys[382] to facilitate toppling of TM10 above Pro[386] (83% conserved) that helps close the external vestibule and allows Gln[378] to approach the other metal-binding residues (Fig. 2*B*).

As expected, mutations to the conserved residues in the metal-binding site (Fig. 2*C*) were all deleterious to Co^{2+} and Mn^{2+} transport (Fig. 2, *D* and *E*), with the exception of Met[230] mutants, which preserved high Co^{2+} transport, as seen previously (4, 19, 21). Serine and asparagine replacements for Gln[378] preserved greater activity than alanine or leucine, indicating the importance of a hydrophilic residue at the position. In addition, the mutations T228A and N426A, which remove the hydrogen bond-donating side chains that support the nonhelical metal-binding region, also impaired transport.

Mutations to the inner-gate polar network impair metal transport

Opening of the interior metal release pathway between TMs 1a, 2, 5, 6b, and 7 proceeds via rearrangements within one of the two networks of highly conserved hydrophilic residues on the cytoplasmic side of the protein (Figs. 1 and 3*E*). In the outward-open structure, Tyr[54] (90% conserved, 10% Phe) acts as a gate by filling the interface among TMs 1a, 2, and 6b and forms a hydrogen-bonding network that includes Gln[89] (100% conserved) and His[237] (93% conserved) (Fig. 3, *A* and *B*). In the inward-occluded state, Tyr[54] is flipped up away from TM6b toward TM7, anchoring a new hydrogen-bonding network that includes Asn[82] (51% conserved), Asn[275] (100% conserved), and Thr[228] (80% conserved) (Fig. 3, *C* and *D*).

Farther below the metal-binding site, in the outward-open state, the Glu[176]-Arg[244] (99% and 84% conserved, respectively) salt bridge tethers TM5 to TM6b, whereas Arg[244] and Asp[263] (75% conserved, 24% Glu) interact with backbone groups to hold TM1a in place (Fig. 3, *A* and *B*). These inner-gate interactions must be disrupted before TM1a swings to fully open the inward metal release pathway. Indeed, they are absent in the inward-occluded (and inward-open) structure (Fig. 3, *C* and *D*), with Glu[176] and Arg[244] ending up 20 Å apart. The invariant Gly[45] presses tightly against the Glu[176]-Arg[244] pair in the outward-open state so that any bulkier residue creates steric clashes. Thus, the G45R mutation precludes proper closing of the inner gate and prevents sampling of the outward-open state (20, 21), explaining the loss-of-function phenotype (20) that causes anemia in humans with the analogous mutation in DMT1 (31).

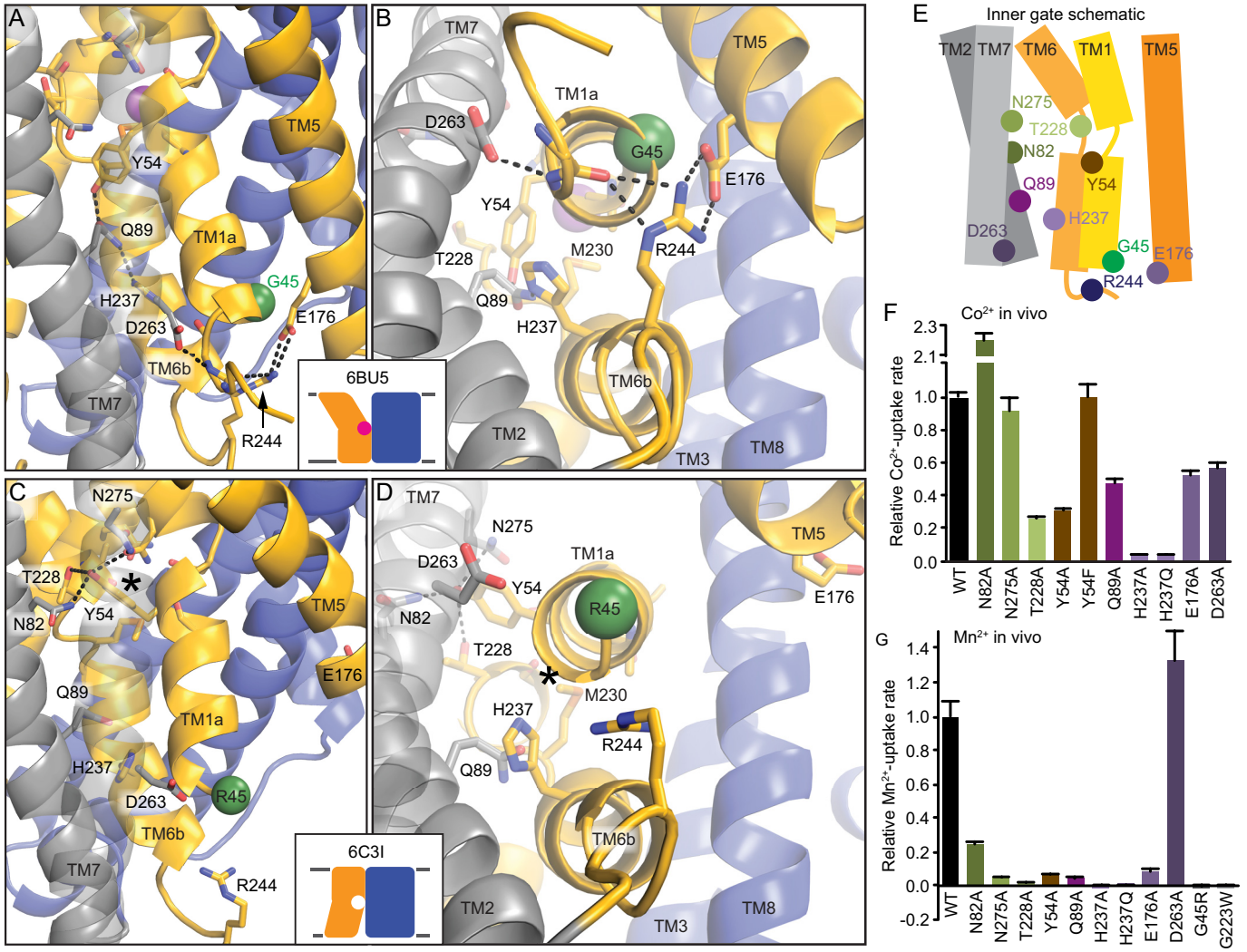

Figure 3. Network of conserved hydrophilic residues rearranges to open intracellular vestibule for metal release. *A* and *B*, conserved hydrophilic interactions close the inner gate in the outward-open structure viewed from the side (*A*) or the intracellular face (*B*). Tyr^{54} forms a gate below the bound metal as part of a network that includes Gln^{89} and His^{237}, whereas lower down, Arg^{244}, Glu^{176}, and Asp^{263} form an extended salt bridge network that helps lock TM1a in place. *C* and *D*, in the inward-occluded structure, viewed from the side (*C*) or the intracellular face (*D*), the lower salt bridge network is disrupted, likely because of the bulky G45R mutation (a *green sphere* shows Cα). Tyr^{54} reorients to interact with Asn^{82}, Thr^{228}, and Asn^{275} and no longer obstructs the metal-binding site from the inside. *E*, schematic of the inner gate network formed by TMs 1a, 2, 5, 6b, and 7. *F* and *G*, most mutations of the hydrophilic gating residues impaired relative *in vivo* Co^{2+} (*F*) and Mn^{2+} (*G*) uptake rates. Data are averages ± S.E. ($n \geq 4$ for Co^{2+} and $n \geq 6$ for Mn^{2+}).

Mutations to these conserved hydrophilic residues involved in opening and closing the inner gate were mostly deleterious to metal transport (Fig. 3, *F* and *G*). However, N275A and Y54F did not significantly reduce, and N82A actually enhanced, the rate of Co^{2+} transport, whereas D263A did not impair Mn^{2+} uptake.

Mutations to the proton transport pathway polar network impair metal transport

Proton transport occurs via a pathway separate from the intracellular metal release route, which remains closed to bulk solvent in proton-transporting, outward-locked mutants (21). On the opposite side of the metal-binding site from Tyr^{54}, which forms the first barrier to metal release, begins a network of highly conserved hydrophilic residues. This network includes at least seven potentially protonatable side chains and leads from proton- and metal-binding Asp^{56} (21) through a tight corridor between TMs 3, 4, 8, and 9 to the cytoplasm (Fig. 4, *A* and *B*) to provide a route for proton transport (4, 21). In contrast to the external and intracellular vestibules proposed as metal entrance and release pathways, the helices and residues within this polar network, with the exception of the cytoplasmic end of TM4, undergo little rearrangement between our outward-open, inward-occluded, and inward-open structures (20, 21).

Highly conserved residues surrounding the metal-binding Asp^{56} includes His^{232} on TM6b (100% conserved) and Glu^{134} (TM3, 98% conserved), which are essential to Nramp proton uniport and proton-metal cotransport (4, 6, 21, 30), along with Thr^{130} (TM3, 69% conserved) and Ser^{327} (TM8, 92% conserved). Across from Glu^{134} lies a conserved salt bridge pair: Asp^{131} (TM3, 93% conserved) and Arg^{353} (TM9, 78% conserved), with Asp^{131}, which is required for proton transport, the likely proton transfer point after incoming metal causes Asp^{56} to deprotonate (4, 21). Approximately 9 Å below, a second conserved salt bridge, Glu^{124}-Arg^{352} (94% and 87% conserved,

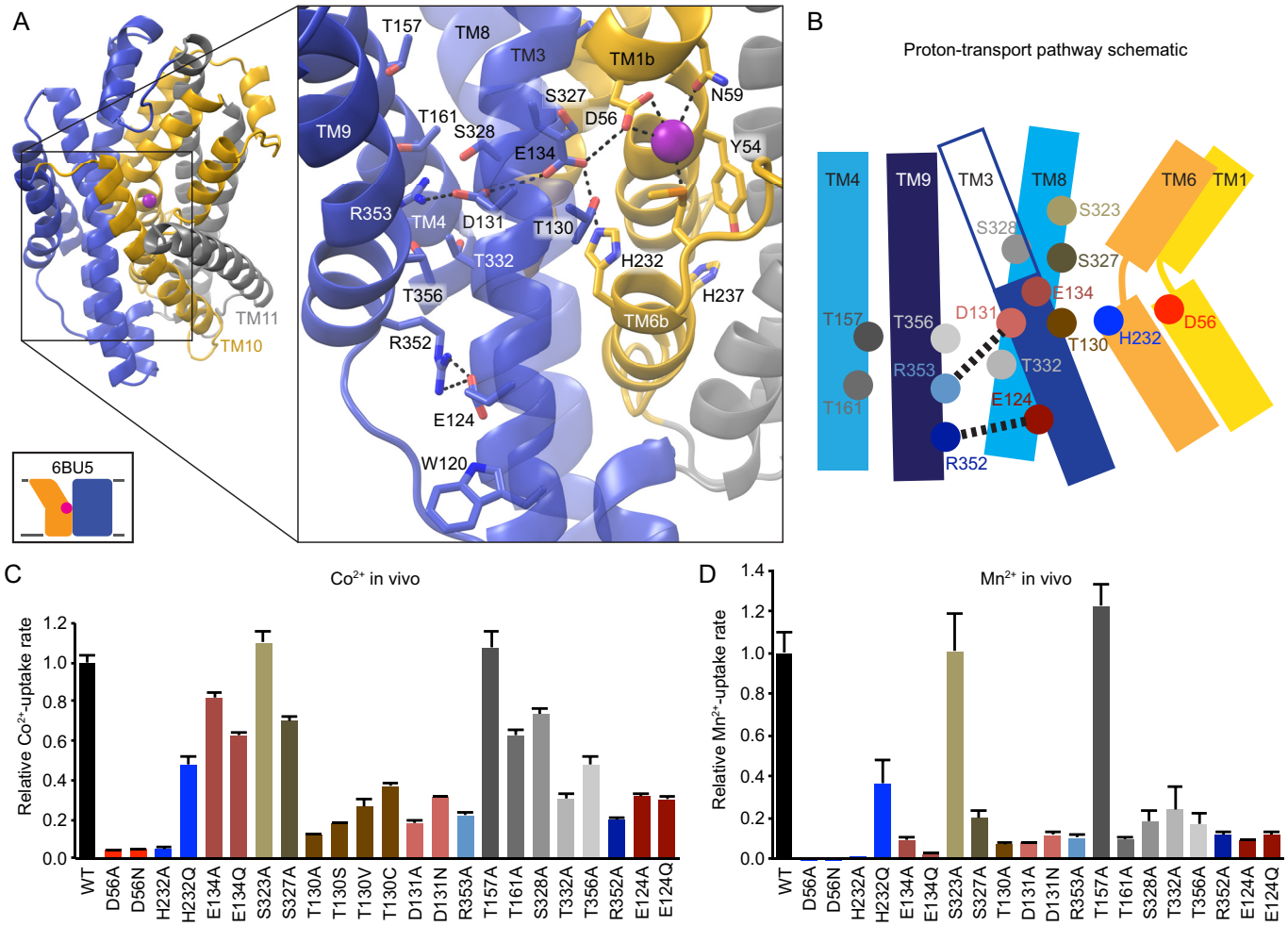

Figure 4. The proton transport pathway leads through a conserved polar network from the metal-binding site to the cytoplasm. *A*, view from an angle above the membrane, looking down into the extracellular vestibule in the outward-open structure, with a magnified *inset* (with TM10 and TM11 omitted for clarity). *B*, schematic showing a network of conserved hydrophilic residues leading from the metal-binding site into the cleft between TMs 3, 4, 8, and 9. His^{232} and Glu^{134} abut metal-binding Met^{230} and Asp^{56}, providing a connection to the Asp^{131}-Arg^{353} and Arg^{352}-Glu^{124} salt bridge pairs. Many moderately conserved hydrophilic residues line the surrounding passageway. *C* and *D*, mutations to many residues in the proton transport pathway impaired relative *in vivo* Co^{2+} (*C*) and Mn^{2+} (*D*) uptake rates. All data are averages ± S.E. ($n \geq 4$ for Co^{2+} and $n \geq 6$ for Mn^{2+}).

respectively), links the same two helices, with several moderately conserved serines and threonines from TMs 4, 8, and 9 in between. Hydrophobic residues around the salt bridge network and below Glu^{124} may help restrict the accessibility of bulk solvent; in previous work, we detected a slight accessibility along that face of TM3 only up to Glu^{124} (20).

Alanine replacement at most positions within this extended polar network generally impaired Co^{2+} and Mn^{2+} transport (Fig. 4, *C* and *D*). Interestingly, alanine replacement of Glu^{134}, essential for voltage dependence and proton–metal coupling (4), preserved significant Co^{2+} uptake, whereas H232A eliminated transport. Thr^{130}, which flanks the interface of the crucial Asp^{56}-Glu^{134}-His^{232}-Met^{230} tetrad along the proton transfer route to Asp^{131}, is particularly important for metal transport, with larger replacements such as T130C preserving greater activity than T130A, indicating that steric bulk here likely aids optimal binding site alignment. Mutations to Ser^{327} and Ser^{328} (20% conserved, 74% Thr), which also line the proton transfer route and may be a remnant of an ancestral Na^+-binding site (21, 32), impaired Mn^{2+} uptake but were less deleterious to Co^{2+} transport. Mutations that disrupt the Glu^{124}-Arg^{352} and Asp^{131}-Arg^{353} salt bridge pairs greatly reduced transport of both substrates. For Thr^{157} (85% conserved), Thr^{161} (35% conserved), Thr^{332} (83% conserved), and Thr^{356} (94% conserved), which cluster between the two TM3-TM9 salt bridges, alanine substitution also impaired transport, but to a lower degree than mutations to the charged residues. Overall, the intact TM3, TM4, TM8, TM9 polar network that provides the proton exit pathway was essential for efficient DraNramp metal transport.

TM6b drives the conformational change required for metal transport

TM6b forms the main structural connection between the two parallel polar networks that diverge from the DraNramp binding site into otherwise distinct structural elements of the protein (Fig. 1). In the outward-open and inward-occluded states, TM6b is closely intertwined with TM1a (21), whereas this interaction is disrupted in the fully inward-open structure (20). Adding steric bulk to positions on TM1a that would prevent the observed tight packing with TM6b eliminated metal transport and locked the transporter in an outward-closed conformation (20). In addition, mutations at several positions on

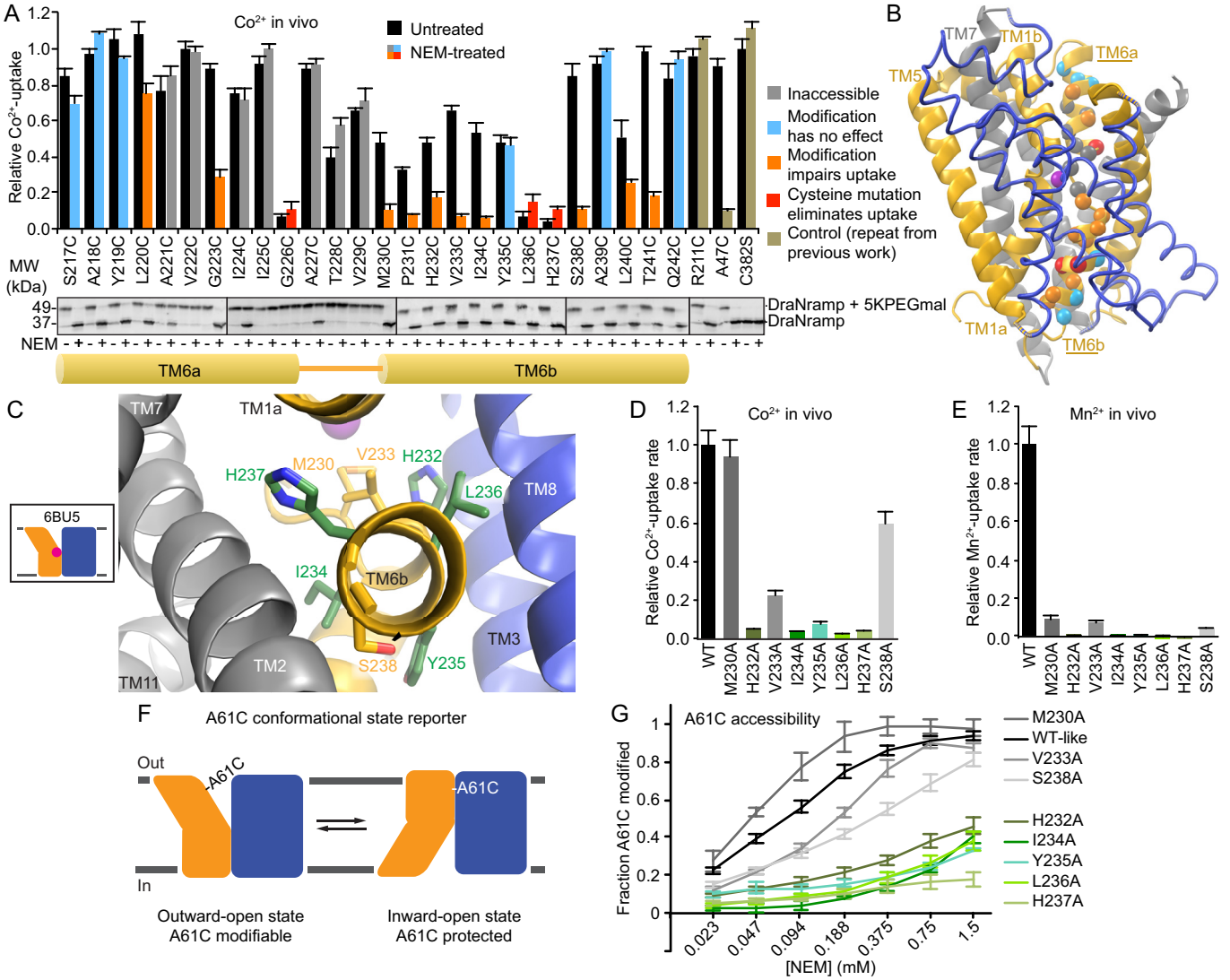

Figure 5. TM6 plays an instrumental role in DraNramp bulk conformational change. *A*, relative *in vivo* Co^{2+} uptake of single-cysteine mutants (which also contain the C382S mutation to remove the lone endogenous cysteine) along TM6 (*black bars*) showed the functional importance of TM6b. Cysteine modification with NEM (*colored bars*) further reduced transport for most positions on TM6b, likely by impeding essential conformational rearrangements. Data are averages ± S.E. ($n = 3$). Western blots indicate which cysteines could be fully modified; preincubation with NEM prevents the upward shift caused by subsequent 5K-PEG maleimide modification under denaturing conditions. *MW*, molecular weight. *B*, the results from *A* mapped onto the outward-open structure to illustrate where NEM modification is tolerated or not. *C*, conserved side chains along TM6b viewed from the cytoplasm. *D* and *E*, alanine scanning of TM6b residues reduced or eliminated relative *in vivo* Co^{2+} (*D*) and Mn^{2+} (*E*) uptake. Data are averages ± S.E. ($n \geq 4$ for Co^{2+} and $n \geq 6$ for Mn^{2+}). *F*, A61C acts as a reporter for sampling of the outward-open state, as this position is fully protected from NEM modification in the inward-open state. *G*, many TM6b alanine mutants protected A61C from NEM modification, indicating an impairment of conformational cycling. *WT-like* refers to the A61C/C382S DraNramp variant. All other variants used to perform these cysteine accessibility experiments also contained the A61C/C382S double mutation, which, as we showed previously, preserves *in vivo* and *in vitro* metal transport at a WT-like level (20, 21). Data are averages ± S.E. ($n \geq 4$).

TM6 impaired high-affinity Mn^{2+} transport in *E. coli* Nramp (33). Based on these previous findings, we postulated that TM6b might play an essential role in corralling TM1a to fully close the metal pathway's inner gate as a prerequisite for opening the external vestibule.

To test this hypothesis, we measured the Co^{2+} transport ability of a panel of single-cysteine mutants spanning TM6 (Fig. 5*A*). Introducing cysteines along TM6a (Ala^{217} to Ala^{227}) did not greatly affect function, except at the invariant Gly^{226}. However, for 10 consecutive positions, from the unwound region at Thr^{228} through the first half of TM6b to His^{237}, cysteine substitution moderately or severely impaired metal transport, particularly at the highly conserved Leu^{236} (93% conserved) and His^{237} (93% conserved). In contrast, cysteine substitution in the second half of TM6b (Ser^{238} to Glu^{242}) did not notably diminish transport, except at Leu^{240}.

Next we investigated the effects of bulky N-ethylmaleimide (NEM) modification along TM6 (Fig. 5, *A* and *B*). Briefly, we used a two-step labeling protocol in which NEM was applied to *E. coli* expressing the single-cysteine DraNramp construct. Cells were then lysed and protein denatured before adding 5K-PEG maleimide to modify previously unlabeled cysteines and cause a gel shift on Western blots. Most positions on TM6a were not full modified, indicating a highly constricted environment. In contrast, all positions from Met^{230} and below were completely NEM-labeled, likely from the protein sampling a

conformational state with a large cytoplasmic aqueous vestibule, as seen in our original inward-open structure (20). Adding the bulky NEM moiety along the external vestibule at Leu^{220} or Gly^{223} impaired metal transport, likely by impeding proper closing of that vestibule, consistent with our previous results for tryptophan substitution at those positions (21). Interestingly, NEM modification further reduced or eliminated Co^{2+} transport for eight positions on TM6b (Met^{230}-Ile^{234}, Ser^{238}, Leu^{240}, and Thr^{241}) but not at Tyr^{235}, Ala^{239}, or Glu^{242} (Fig. 5, *A* and *B*). Those latter positions face the scaffold domain (TM3 and TM8). These results suggest that the lower part of TM6b (Tyr^{235} and below) does not snugly interact with TM3 and TM8 (which, along with TM4 and TM9, form the pathway for proton transport (21)) in any essential conformation. However, on all other sides of TM6b, which face TMs 1a, 2, 7, and 10, NEM modification eliminated any residual Co^{2+} transport, likely because the adduct created steric clashes that block essential conformational rearrangements, such as inward movement of TM1a. Thus, although TM6b itself does not reorient dramatically in our prior crystal structures, it may form a nexus for the rearrangements of other essential moving parts in the DraNramp transport cycle or else move significantly itself in an as-yet-uncaptured conformational state.

To further understand the role of TM6b, we measured Co^{2+} and Mn^{2+} transport for a panel of alanine substitutions from Met^{230}-Ser^{238} (Fig. 5, *C–E*). For this panel, we also measured A61C accessibility to assess the mutants' conformational cycling ability (Fig. 5, *F* and *G*); this single cysteine reporter on TM1b is only accessible to NEM modification in DraNramp's outward-open conformation (20, 21). Most mutations removing bulky side chains (H232A, I234A, Y235A, L236A, and H237A) reduced sampling of the outward-open state and impaired or eliminated metal transport. In contrast with our prior observations regarding TM1a (20), not only adding bulk but also removing bulk from TM6b prevented the conformational change needed for metal transport, underscoring the role its mixture of hydrophilic and hydrophobic residues likely plays in stabilizing helix packing. The native residues of TM6b may therefore assist with closing of the intracellular vestibule, which is likely a prerequisite process for opening of the external vestibule to reach the outward-open state.

TM6b histidines link substrate release pathways to drive conformational change

The clearest structural connection between the two polar networks that form the adjacent intracellular metal and proton release pathways is TM6b, on which His^{232} and His^{237} occupy opposite faces of a highly conserved helix below the metal-binding site (Figs. 5*C* and 6*A*). Others have argued that His^{232} or His^{237} or both have roles in metal binding, proton transport, and/or pH regulation in various Nramp homologs (6, 34–36). His^{232}'s position at the protein core renders it unsuitable for direct protonation, as the congested environment disfavors a net charge on the imidazole (21, 30). This residue is nevertheless essential for high-affinity Mn^{2+} transport, H^+ uniport, and proton–metal cotransport in DraNramp (4, 21) and *Eremococcus coleocola* Nramp (6). We previously proposed that it plays a key role, along with the adjacent Glu^{134}, in stabilizing a proton transfer from Asp^{56} to Asp^{131} (4). His^{237}, located two helical turns more intracellular on TM6b from the metal-binding Met^{230}, is quite distant from the metal-binding site (13.4 Å from the bound Mn^{2+} in the outward-open state) on the TM6b face most distant from the proton release pathway.

Given the many prior studies indicating the importance of these histidines to metal uptake across multiple Nramp homologs and the associated speculation about their function in the transport mechanism (6, 33–36), we tested Co^{2+} transport and A61C accessibility for a variety of side-chain replacements at His^{232} and His^{237} in DraNramp (Fig. 6, *B* and *C*). All tested His^{237} substitutions yielded inward-locked transporters that did not transport metal (Fig. 6, *B* and *C*), illustrating that residue's indispensable role in stabilizing the outward-open state. An alanine substitution of the invariant Glu^{89}, the His^{237} hydrogen bond partner in the outward-open state, had similar but less severe effects.

For His^{232}, the results varied, although all tested mutants besides H232Q profoundly impaired metal transport (Fig. 6*B*). H232N and H232Q slightly increased and decreased A61C accessibility, respectively, whereas H232R locked the transporter in an outward-closed state (Fig. 6*C*). Surprisingly, NEM labeling at A61C of H232F and H232Y matched or exceeded that of the WT at low NEM concentrations but then plateaued at only ~50% and ~25% respectively, whereas A61C labeling of the WT reached completion (Fig. 6*C*). One interpretation of this result is that the H232F and H232Y variants were trapped in a mixture of inward- and outward-open states, with an energy barrier too high for rapid interconversion, explaining the lack of metal transport. Interestingly, the M230T/H232Y double substitution, which changes the TM6 MPH motif to the TPY found in Nramp-related Mg^{2+} and Al^{3+} transporters (37, 38), may relieve this jam, as it partially restored both A61C labeling and metal transport (Fig. 6, *B* and *C*), emphasizing the structural and functional connection between His^{232} position and the metal-binding site. This conserved histidine lies at the interface of the mobile and scaffold regions of the protein along the proton pathway and thus could serve as a pivot point for bulk conformational change upon sensing metal binding or proton transfer.

Discussion

Previously, we demonstrated the importance of alternating-access conformational changes to Nramp metal transport (20, 21) and elucidated the role of a conserved salt bridge network in enabling proton uniport and proton–metal cotransport (4, 21). Here we illustrated the importance of two parallel cytoplasmic networks of conserved hydrophilic residues in *in vivo* DraNramp metal transport (Fig. 7). One polar network extends below the metal-binding site to form an inner gate that rearranges to allow metal release in the inward-open state (Fig. 3). A second polar network encapsulates the essential salt bridge network and provides a route for proton exit to the cytoplasm (Fig. 4). The highly conserved TM6b, which forms the structural link between these two networks, is essential for the conformational change process (Fig. 5). TM6b's two conserved histidines, His^{232} and His^{237}, are important in control of the transporter's conformational state (Fig. 6) and likely are instrumental in driv-

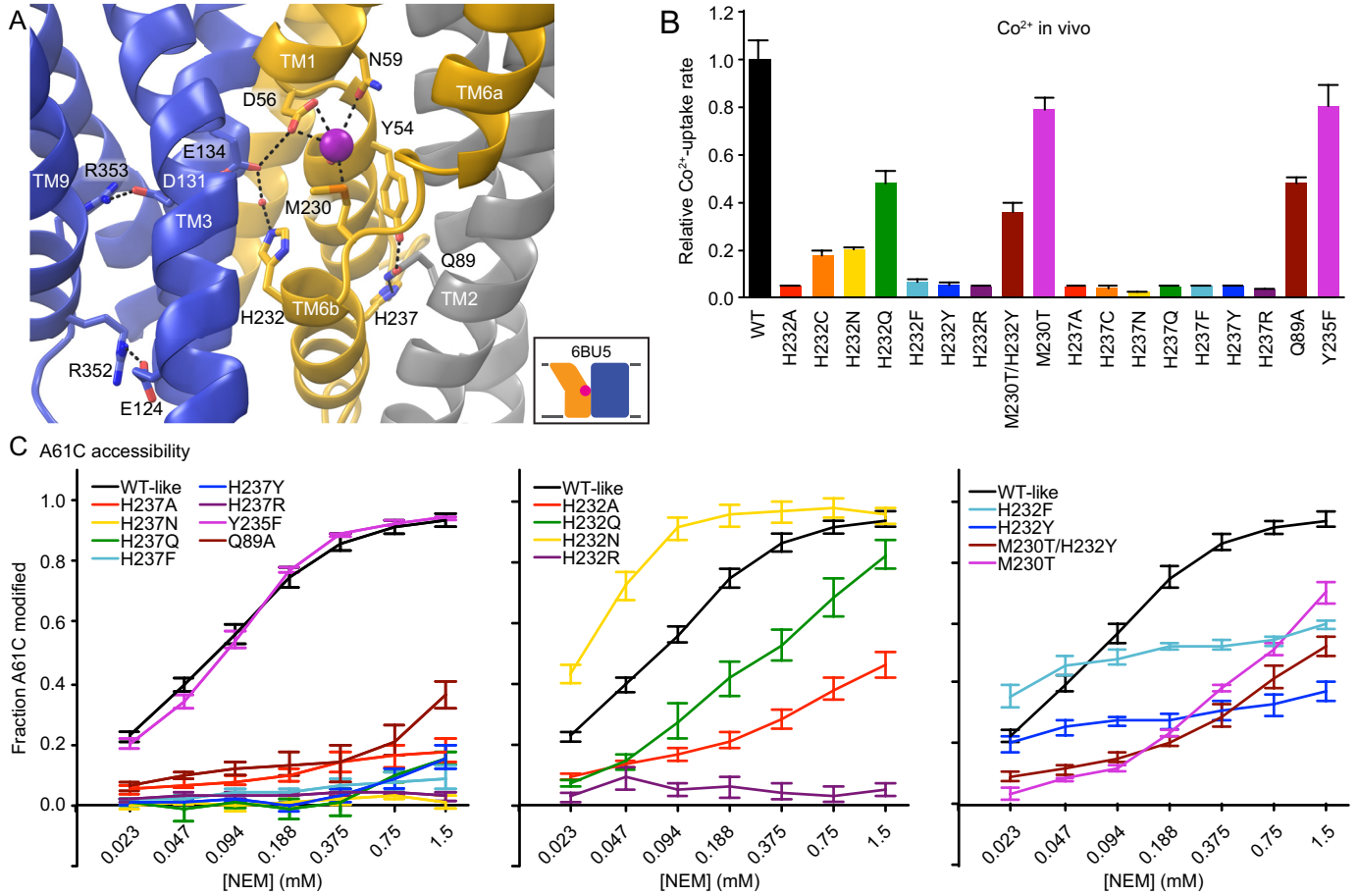

Figure 6. TM6 histidines govern the DraNramp conformational state. *A*, view from the periplasm of outward-open DraNramp, highlighting the key positions of His^{232} and His^{237} in relation to the metal-binding site and proton transport pathway. For clarity, TMs 10 and 11 were removed. *B*, all tested mutations to His^{232} impaired relative *in vivo* Co^{2+} uptake rates, with H232Q the only significantly active mutant. All tested mutations to His^{237} eliminated relative *in vivo* Co^{2+} uptake. *C*, NEM accessibility experiments showed all mutations to His^{237} rendered A61C fully protected, indicating an outward-closed state. Mutations to His^{232} perturbed A61C accessibility, indicating disparate effects on the conformational equilibrium. All data are averages ± S.E. ($n \geq 4$).

ing the switch to the inward-open state upon metal binding (His^{232}) and promoting the return of the empty carrier to the outward-open state after metal release (His^{237}). Several conserved hydrophobic residues, including Ile^{234} and Leu^{236} (Fig. S1), likely contribute important hydrophobic packing interactions to the process. Our findings suggest that TM6b serves to link Nramp metal and proton binding and/or release to bulk conformational change to achieve alternating-access metal transport. In this model, TM6b may be the structural lynchpin underlying Nramp's unconventional cotransport mechanism, in which metal and protons take separate pathways to reach the cytoplasm to avoid like-charge repulsion (4, 21) and yet manage to remain at least loosely coupled (8).

The inherent asymmetry of Nramps (a hydrophobic outer gate and two hydrophilic cytoplasmic networks, one forming the inner gate for metal release and the second forming a parallel proton transport pathway) may be an evolutionary adaptation to promote outside-to-inside transport. The hydrophilic inner gate residues may position water molecules to facilitate eventual metal rehydration and release upon conformational change, and we observed just such an ordered water tethered by His^{232} in our outward-open structure (Fig. 6*A*) (21). In contrast, the hydrophobic packing above the metal-binding site should prevent any similar assistance in the reverse direction, guarding against metal efflux. In addition, there is no structural equivalent to the parallel proton transport network in the external half of the protein, which provides spatial separation of the two like-charge cosubstrates during the transport process from outside to inside (4, 21).

Our functional data in Fig. 5 indicate an essential role for TM6b in conformational change and metal transport not yet captured by crystallography. Superpositions of the available DraNramp crystal structures did not reveal significant displacement of TM6b in the conformational change from outward-open to inward-occluded (Cα root mean square deviation of 0.7 Å) (21). Although a slightly larger difference was seen from inward-occluded to inward-open (Cα root mean square deviation of 2.1 Å), the electron density for the lower half of TM6b (below Leu^{236}) was not well resolved in the inward-open structure (21). Analogous structural comparisons of the inward-open *S. capitis* Nramp (34% identical/56% similar to DraNramp) and the outward-open *E. coleocola* Nramp (33% identical/52% similar to DraNramp, 47% identical/64% similar to *S. capitis* Nramp) also indicated little displacement of TM6b (6). As bulky modification on TM6b facing TMs 1a, 2, 7, and 10 (Fig. 5, *A* and *B*) eliminated metal transport, perhaps those helices reorient significantly relative to TM6b. However, both structural superpositions and distance difference matrix calcu-

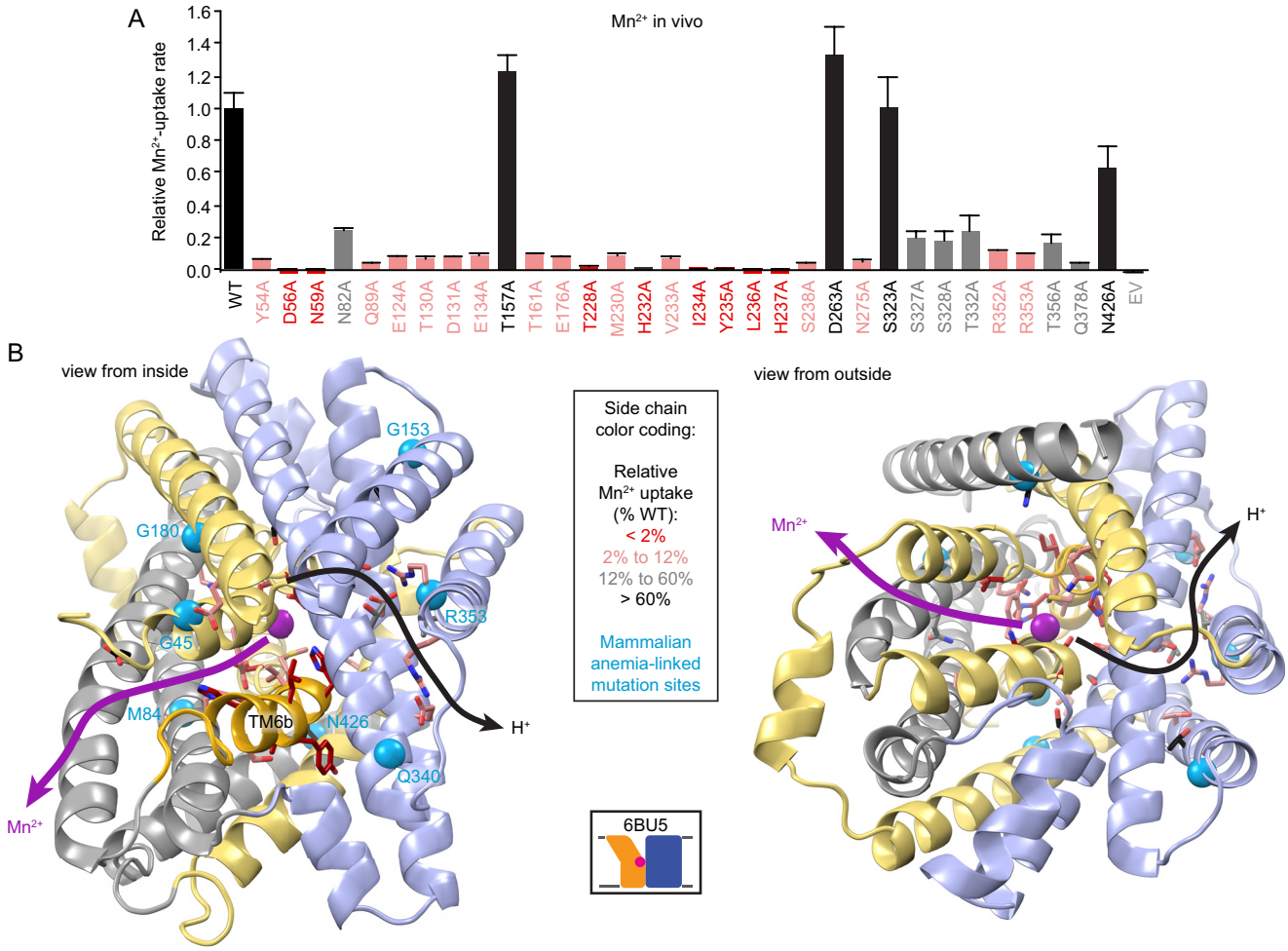

Figure 7. TM6b links two conserved polar networks. *A*, Mn^{2+} uptake data for a DraNramp alanine mutant panel. Data are averages ± S.E. ($n \geq 6$), repeated from Figs. 2–5. *B*, DraNramp outward-open structure, showing side chains of tested residues as *sticks* color-coded by the severity of Mn^{2+} transport impairment caused by mutation to alanine. TM6b is highlighted in *deeper yellow*. Seven mammalian anemia-causing mutations are indicated as *cyan spheres*. The proposed separate pathways for Mn^{2+} and H^+ transport to the cytoplasm are shown as *arrows*.

lations revealed little relative displacement between TMs 6b and TM2, 7, or 10 (21), which *S. capitis* and *E. coleocola* Nramp comparisons also corroborated (6). In contrast, our analyses did highlight the ~45° displacement of TM1a in the inward-open state compared with its position in the inward-occluded and outward-open states (21). As would be expected, adding steric bulk on TM1a eliminated metal transport and trapped the protein in an outward-closed conformation, validating the functional importance of TM1a's movement (20). The similar functional results with TM6b therefore suggest a significant displacement for that helix at some point in the transport cycle.

Previous work with the distantly related structural homolog LeuT, a Na^+-driven amino acid transporter, supports the likelihood of an essential TM6b motion not apparent from crystal structures. Comparisons of LeuT in inward- and outward-open states showed little displacement of TM6b or the neighboring parts of TMs 2, 7, and 10 (6, 39). However, double electron–electron resonance measurements with LeuT indicated significant motion of TM6b (and TM7) between conformational states, likely as part of opening and closing the inner gate (40). In addition, molecular dynamics simulations with LeuT showed more substantial rearrangements for TM6b during substrate release (41, 42), with TM6b perhaps also serving to allosterically link substrate binding to the opening of the inner gate (43). Cysteine modification experiments (44) and molecular dynamics simulations (45) with LeuT's close homologs corroborate TM6b's importance to conformational change. In addition, mutation to alanine of a highly conserved tyrosine on TM6b, which disrupts a hydrophilic inner gate network, caused the protein to relax into the inward-open state, as captured in the crystal structure (39) and confirmed with FRET (46) and double electron–electron resonance data (40). Similarly, mutation of a TM6b phenylalanine at the bottom of the substrate binding site in LeuT also altered the relative substrate specificity and the conformational preferences of the transporter (47). These observations echo our previous finding in DraNramp that the analogously located Met^{230} contributes to a metal selectivity filter (19) as well as our current results regarding how mutations to His^{232} (located on the same face of TM6b just below Met^{230}) tune the conformational state preferences of DraNramp (Fig. 6). The many apparent similarities between TM6b in DraNramp and LeuT may reflect an already evolved functional role of this helix in the ancestral precursor to both transporters, which was then preserved through the divergence

of other conformational rearrangements as well as their substrate type and coupling mechanism.

Nramp crystal structures of *S. capitis* and *E. coleocola* homologs revealed polar networks analogous to those seen in DraNramp (6, 27). In addition, previous functional studies with the *E. coli* homolog (51% identical and 72% similar to DraNramp) confirmed the importance of the conserved polar networks and TM6b to the transport mechanism. Two studies (33, 48) showed deleterious effects for mutations to Asp^{34} (Asp^{56} in DraNramp), Pro^{35} (Pro^{57}), Gly^{36} (Gly^{58}), Asn^{37} (Asn^{59}), Gly^{205} (Gly^{226}), Ala^{206} (Ala^{227}), and Met^{209} (Met^{230}) within the metal-binding site region; Glu^{154} (Glu^{176}) and Asp^{238} (Asp^{263}) within the inner gate network; Glu^{102} (Glu^{124}), Asp^{109} (Asp^{131}), and Glu^{112} (Glu^{134}) in the proton transport pathway; and Pro^{210} (Pro^{231}), His^{211} (His^{232}), Leu^{215} (Leu^{236}), His^{216} (His^{237}), and Ser^{217} (Ser^{238}) on TM6b, which the authors also proposed as a likely key player in the conformational change process (33). Two additional studies (34, 49) showed that mutations to the aforementioned Asp^{34}, Asn^{37}, His^{211}, and His^{216} impaired metal uptake, as did mutations to Asn^{250} (Asn^{275}) in the inner gate network and Asn^{401} (Asn^{426}) in the unwound region. Additionally, many of these conserved residues have also been shown to be important to metal transport in *Arabidopsis thaliana* Nramp3 (50).

Interestingly, mammalian anemia-causing DMT1 mutations cluster within the two identified polar networks (Fig. 7*B*). The human DMT1 (26% identical, 48% similar to DraNramp) mutant N491S (Asn^{426} in DraNramp) (51) truncates the asparagine that differentially stabilizes the nonhelical metal-binding site region (Fig. 2). The ΔV114 (Met^{84}) (52) mutation shifts the registry of TM2 within the protein's metal release pathway. The mutants G75R (Gly^{45}) on TM1a (31) and G212V (Gly^{180}) on TM5 (52) in human DMT1 add steric bulk at positions abutting the highly conserved Glu^{176}-Arg^{244} salt bridge, which forms part of the inner gate that closes the metal-release pathway in the outward-open state (Fig. 3). In addition, the human DMT1 mutant R416C (Arg^{353}) on TM9 (53, 54) removes a highly conserved charged residue from the proton transport pathway, whereas the mouse and rat DMT1 mutant G185R (Gly^{153}) on TM4 (13, 55) adds an additional positive charge in the vicinity of that network (Fig. 4). The human DMT1 mutant E399D (Gln^{340}) on TM8 (52), which makes a conservative substitution in the proton transport pathway polar network, preserved metal transport function (56).

In addition, designed mammalian DMT1 mutants to Asp^{86} (Asp^{56}, TM1) (19, 27, 35), Asn^{89} (Asn^{59}, TM1) (27), Met^{265} (Met^{230}, TM6) (19, 27, 30), and Asn^{443} (Gln^{378},TM10) (30) in the metal-binding site disrupted metal transport, as did mutations to Glu^{154} (Glu^{124}, TM3) (35), Asp^{161} (Asp^{131}, TM3) (35), Glu^{164} (Glu^{134}, TM3) (30), and Arg^{416} (Arg^{353}, TM9) (35, 54) in the proton transport pathway. The TM6b histidines His^{267} (His^{232}) and His^{272} (His^{237}) were the focus of two prior studies (35, 36). One showed that lowering the external pH rescued some Fe^{2+} transport activity for H267A/C and H272A/C mutants but not for H267R and H272R replacements, which lacked any activity (35). The authors proposed that these residues directly protonate/deprotonate to regulate transport and conformational change. An alternative explanation consistent with our DraNramp findings is that, although the bulky arginine replacements trap the transporter in an inward-locked conformation that prevents transport, the smaller replacements simply shift the conformational equilibrium to disfavor the outward-open state. If a protonation event perhaps stabilizes human DMT1's outward-open state analogously to how Na^+ binding stabilizes LeuT's outward-open conformation (57, 58), then lowering the external pH might compensate some for the H267A/C and H272A/C mutants, explaining the partial functional recovery. The second study showed a similar reduction of Fe^{2+} transport for H267A/N/D and H272R mutants but obtained more complicated results with H272A (36). The latter mutant altered relative metal preferences to favor Zn^{2+}, eliminated ΔpH stimulation of Fe^{2+} transport, increased the rate of proton uniport, and decoupled cotransport so that adding Fe^{2+} inhibited rather than stimulated H^+ influx (36). The broad effects of H272A in mammalian DMT1 echo the results of perturbing the TM3-TM9 salt bridge network, which alter the voltage and ΔpH dependence of the metal transport rate as well as proton–metal cotransport stoichiometry in DraNramp (4, 21), suggesting that this residue may have an additional essential mechanistic role beyond closing the inner gate to stabilize the outward-open state, at least in some Nramp homologs.

The two identified cytoplasmic polar networks that provide the pathways for metal release and proton transport and the highly conserved TM6b that connects them are thus clearly essential for proper function of our model system DraNramp as well as *E. coli* Nramp and mammalian DMT1. In particular, our results here, in combination with previously published structural and biochemical data, clearly establish that the integrity of TM6b is crucial for proper conformational cycling required for efficient import of transition metals into the cytosol by Nramp transporters.

Experimental procedures

Cloning of DraNramp

WT and mutant DraNramps were cloned in pET21-N8H as described (20). For the manganese uptake assay, the fluorescent Ca^{2+}-sensor GCaMP6f (59) was inserted into pETDuet in the first multiple cloning site using NcoI and NotI cut sites. WT DraNramp and point mutants were inserted into the second multiple cloning site of pETDuet using NdeI and XhoI cut sites, with the vector modified to insert an N-terminal His_8 tag that ends in the NdeI site. Mutations were made using the QuikChange mutagenesis protocol (Stratagene) and confirmed by DNA sequencing. Single-cysteine constructs also included the C382S mutation to remove the lone endogenous cysteine. The C41(DE3) *E. coli* strain was used for protein expression and *in vivo* assays.

In vivo metal transport assays

Cobalt uptake assays in *E. coli* were performed as described previously (19, 20). For cysteine premodification experiments, cells were plated, incubated in labeling buffer (100 mM Tris (pH 7.0), 60 mM NaCl, 10 mM KCl, 0.5 mM $MgCl_2$, and 0.75 mM $CaCl_2$) with or without 3 mM NEM for 15 min at room temperature, quenched with 10 μl of 200 mM L-cysteine, and then

washed twice in assay buffer before assaying metal uptake. To measure relative rates of manganese uptake, DraNramp and the fluorescent Ca^{2+} sensor GCaMP6f (59) were coexpressed. The metal-binding EF-hand domain of calmodulin that comprises the Ca^{2+} sensor in GCaMP6f also binds Mn^{2+} in the same two binding sites as Ca^{2+}, with a slightly different coordination geometry and at an ~2-fold lower affinity (K_D = 13 μM) (60). For this assay, 15 ml of lysogeny broth and 100 μg/ml ampicillin were seeded 1/50 from overnight cultures. Cells were grown at 37 °C until optical density ≈ 0.6 and then induced with 100 μM isopropyl 1-thio-β-D-galactopyranoside and 150 μM EDTA (to sequester trace Mn^{2+} in the medium), with protein expression continuing for 2.5 h at 37 °C. Cells were pelleted and washed twice with assay buffer (50 mM HEPES (pH 7.3), 60 mM NaCl, 10 mM KCl, 0.5 mM $MgCl_2$, and 0.217% glucose) and resuspended at optical density = 5.26 in assay buffer. Cells were plated at 190 μl/well into black clear-bottom plates (Greiner). Baseline fluorescence ($\lambda_{excitation}$ = 470 nm, $\lambda_{emission}$ = 520 nm) was measured on a FlexStation3 (Molecular Devices) for 1 min before 10 μl of 2 mM $MnCl_2$ was added (100 μM final concentration), and fluorescence was measured for another 4 min at room temperature (Fig. S3). To determine the maximum fluorescence signal, 10 mM $CaCl_2$ was added to separate 190-μl aliquots of each mutant and the end-point fluorescence was recorded after a 7-min incubation. To calculate relative manganese uptake, the premetal addition baseline average fluorescence was subtracted from all time points, with the residual fluorescence then divided by the corresponding maximum fluorescence increase in the presence of Ca^{2+}. Average initial rates were normalized to the WT.

Cysteine accessibility measurements

Cysteine accessibility measurements were performed as described previously (20, 21).

Author contributions—A. T. B. and R. G. conceptualization; A. T. B. and R. G. data curation; A. T. B. formal analysis; A. T. B. and R. G. validation; A. T. B., A. L. M., B. C. B., and R. G. investigation; A. T. B. and R. G. visualization; A. T. B., A. L. M., B. C. B., and R. G. methodology; A. T. B. writing-original draft; A. T. B., A. L. M., B. C. B., and R. G. writing-review and editing; R. G. resources; R. G. supervision; R. G. funding acquisition; R. G. project administration.

Acknowledgments—We thank Wilhelm Weihofen, Lukas Bane, Christina Zimanyi, Jack Nicoludis, and other Gaudet laboratory members for helpful discussions.

References

1. Waldron, K. J., Rutherford, J. C., Ford, D., and Robinson, N. J. (2009) Metalloproteins and metal sensing. *Nature* **460,** 823–830 CrossRef Medline
2. Chandrangsu, P., Rensing, C., and Helmann, J. D. (2017) Metal homeostasis and resistance in bacteria. *Nat. Rev. Microbiol.* **15,** 338–350 CrossRef Medline
3. Finney, L. A., and O'Halloran, T. V. (2003) Transition metal speciation in the cell: insights from the chemistry of metal ion receptors. *Science* **300,** 931–936 CrossRef Medline
4. Bozzi, A. T., Bane, L. B., Zimanyi, C. M., and Gaudet, R. (2019) Unique structural features in an Nramp metal transporter impart substrate-specific proton cotransport and a kinetic bias to favor import. *J. Gen. Physiol.* **151,** 1413–1429 CrossRef Medline
5. Chen, X. Z., Peng, J. B., Cohen, A., Nelson, H., Nelson, N., and Hediger, M. A. (1999) Yeast SMF1 mediates H^+-coupled iron uptake with concomitant uncoupled cation currents. *J. Biol. Chem.* **274,** 35089–35094 CrossRef Medline
6. Ehrnstorfer, I. A., Manatschal, C., Arnold, F. M., Laederach, J., and Dutzler, R. (2017) Structural and mechanistic basis of proton-coupled metal ion transport in the SLC11/NRAMP family. *Nat. Commun.* **8,** 14033 CrossRef Medline
7. Gunshin, H., Mackenzie, B., Berger, U. V., Gunshin, Y., Romero, M. F., Boron, W. F., Nussberger, S., Gollan, J. L., and Hediger, M. A. (1997) Cloning and characterization of a mammalian proton-coupled metal-ion transporter. *Nature* **388,** 482–488 CrossRef Medline
8. Rudnick, G. (2019) Unconventional transport of metal ions and protons by Nramps. *J. Gen. Physiol.* **151,** 1339–1342 CrossRef Medline
9. Makui, H., Roig, E., Cole, S. T., Helmann, J. D., Gros, P., and Cellier, M. F. (2000) Identification of the *Escherichia coli* K-12 Nramp orthologue (MntH) as a selective divalent metal ion transporter. *Mol. Microbiol.* **35,** 1065–1078 CrossRef Medline
10. Thomine, S., Wang, R., Ward, J. M., Crawford, N. M., and Schroeder, J. I. (2000) Cadmium and iron transport by members of a plant metal transporter family in *Arabidopsis* with homology to Nramp genes. *Proc. Natl. Acad. Sci. U.S.A.* **97,** 4991–4996 CrossRef Medline
11. Cohen, A., Nelson, H., and Nelson, N. (2000) The family of SMF metal ion transporters in yeast cells. *J. Biol. Chem.* **275,** 33388–33394 CrossRef Medline
12. Canonne-Hergaux, F., Gruenheid, S., Ponka, P., and Gros, P. (1999) Cellular and subcellular localization of the Nramp2 iron transporter in the intestinal brush border and regulation by dietary iron. *Blood* **93,** 4406–4417 CrossRef Medline
13. Fleming, M. D., Trenor, C. C., 3rd, Su, M. A., Foernzler, D., Beier, D. R., Dietrich, W. F., and Andrews, N. C. (1997) Microcytic anaemia mice have a mutation in Nramp2, a candidate iron transporter gene. *Nat. Genet.* **16,** 383–386 CrossRef Medline
14. Gruenheid, S., Canonne-Hergaux, F., Gauthier, S., Hackam, D. J., Grinstein, S., and Gros, P. (1999) The iron transport protein NRAMP2 is an integral membrane glycoprotein that colocalizes with transferrin in recycling endosomes. *J. Exp. Med.* **189,** 831–841 CrossRef Medline
15. Hubert, N., and Hentze, M. W. (2002) Previously uncharacterized isoforms of divalent metal transporter (DMT)-1: implications for regulation and cellular function. *Proc. Natl. Acad. Sci. U.S.A.* **99,** 12345–12350 CrossRef Medline
16. Cunrath, O., and Bumann, D. (2019) Host resistance factor SLC11A1 restricts *Salmonella* growth through magnesium deprivation. *Science* **366,** 995–999 CrossRef Medline
17. Govoni, G., Canonne-Hergaux, F., Pfeifer, C. G., Marcus, S. L., Mills, S. D., Hackam, D. J., Grinstein, S., Malo, D., Finlay, B. B., and Gros, P. (1999) Functional expression of Nramp1 *in vitro* in the murine macrophage line RAW264.7. *Infect. Immun.* **67,** 2225–2232 CrossRef Medline
18. Jabado, N., Jankowski, A., Dougaparsad, S., Picard, V., Grinstein, S., and Gros, P. (2000) Natural resistance to intracellular infections: natural resistance-associated macrophage protein 1 (Nramp1) functions as a pH-dependent manganese transporter at the phagosomal membrane. *J. Exp. Med.* **192,** 1237–1248 CrossRef Medline
19. Bozzi, A. T., Bane, L. B., Weihofen, W. A., McCabe, A. L., Singharoy, A., Chipot, C. J., Schulten, K., and Gaudet, R. (2016) Conserved methionine dictates substrate preference in Nramp-family divalent metal transporters. *Proc. Natl. Acad. Sci. U.S.A.* **113,** 10310–10315 CrossRef Medline
20. Bozzi, A. T., Bane, L. B., Weihofen, W. A., Singharoy, A., Guillen, E. R., Ploegh, H. L., Schulten, K., and Gaudet, R. (2016) Crystal structure and conformational change mechanism of a bacterial nramp-family divalent metal transporter. *Structure* **24,** 2102–2114 CrossRef Medline
21. Bozzi, A. T., Zimanyi, C. M., Nicoludis, J. M., Lee, B. K., Zhang, C. H., and Gaudet, R. (2019) Structures in multiple conformations reveal distinct transition metal and proton pathways in an Nramp transporter. *eLife* **8,** e41124 CrossRef Medline

22. Shu, H. Y., and Tian, B. M. (2010) Function analysis of two Mn(II) ion transporter genes (DR1709 and DR2523) in *Deinococcus radiodurans*. *African Journal of Biotechnology* **9,** 2742–2747
23. Sun, H., Li, M., Xu, G., Chen, H., Jiao, J., Tian, B., Wang, L., and Hua, Y. (2012) Regulation of MntH by a dual Mn(II)- and Fe(II)-dependent transcriptional repressor (DR2539) in *Deinococcus radiodurans*. *PLoS ONE* **7,** e35057 CrossRef Medline
24. Daly, M. J., Gaidamakova, E. K., Matrosova, V. Y., Vasilenko, A., Zhai, M., Venkateswaran, A., Hess, M., Omelchenko, M. V., Kostandarithes, H. M., Makarova, K. S., Wackett, L. P., Fredrickson, J. K., and Ghosal, D. (2004) Accumulation of Mn(II) in *Deinococcus radiodurans* facilitates γ-radiation resistance. *Science* **306,** 1025–1028 CrossRef Medline
25. Forrest, L. R., Krämer, R., and Ziegler, C. (2011) The structural basis of secondary active transport mechanisms. *Biochim. Biophys. Acta* **1807,** 167–188 CrossRef Medline
26. Forrest, L. R., and Rudnick, G. (2009) The rocking bundle: a mechanism for ion-coupled solute flux by symmetrical transporters. *Physiology* **24,** 377–386 CrossRef Medline
27. Ehrnstorfer, I. A., Geertsma, E. R., Pardon, E., Steyaert, J., and Dutzler, R. (2014) Crystal structure of a SLC11 (NRAMP) transporter reveals the basis for transition-metal ion transport. *Nat. Struct. Mol. Biol.* **21,** 990–996 CrossRef Medline
28. Shimamura, T., Weyand, S., Beckstein, O., Rutherford, N. G., Hadden, J. M., Sharples, D., Sansom, M. S., Iwata, S., Henderson, P. J., and Cameron, A. D. (2010) Molecular basis of alternating access membrane transport by the sodium-hydantoin transporter Mhp1. *Science* **328,** 470–473 CrossRef Medline
29. Yamashita, A., Singh, S. K., Kawate, T., Jin, Y., and Gouaux, E. (2005) Crystal structure of a bacterial homologue of Na^+/Cl^--dependent neurotransmitter transporters. *Nature* **437,** 215–223 CrossRef Medline
30. Pujol-Giménez, J., Hediger, M. A., and Gyimesi, G. (2017) A novel proton transfer mechanism in the SLC11 family of divalent metal ion transporters. *Sci. Rep.* **7,** 6194 CrossRef Medline
31. Blanco, E., Kannengiesser, C., Grandchamp, B., Tasso, M., and Beaumont, C. (2009) Not all DMT1 mutations lead to iron overload. *Blood Cells Mol. Dis.* **43,** 199–201 CrossRef Medline
32. Perez, C., and Ziegler, C. (2013) Mechanistic aspects of sodium-binding sites in LeuT-like fold symporters. *Biol. Chem.* **394,** 641–648 CrossRef Medline
33. Haemig, H. A., Moen, P. J., and Brooker, R. J. (2010) Evidence that highly conserved residues of transmembrane segment 6 of *Escherichia coli* MntH are important for transport activity. *Biochemistry* **49,** 4662–4671 CrossRef Medline
34. Courville, P., Urbankova, E., Rensing, C., Chaloupka, R., Quick, M., and Cellier, M. F. (2008) Solute carrier 11 cation symport requires distinct residues in transmembrane helices 1 and 6. *J. Biol. Chem.* **283,** 9651–9658 CrossRef Medline
35. Lam-Yuk-Tseung, S., Govoni, G., Forbes, J., and Gros, P. (2003) Iron transport by Nramp2/DMT1: pH regulation of transport by 2 histidines in transmembrane domain 6. *Blood* **101,** 3699–3707 CrossRef Medline
36. Mackenzie, B., Ujwal, M. L., Chang, M. H., Romero, M. F., and Hediger, M. A. (2006) Divalent metal-ion transporter DMT1 mediates both H^+-coupled Fe^{2+} transport and uncoupled fluxes. *Pflugers Arch.* **451,** 544–558 CrossRef Medline
37. Shin, J. H., Wakeman, C. A., Goodson, J. R., Rodionov, D. A., Freedman, B. G., Senger, R. S., and Winkler, W. C. (2014) Transport of magnesium by a bacterial Nramp-related gene. *PLoS Genet.* **10,** e1004429 CrossRef Medline
38. Xia, J., Yamaji, N., Kasai, T., and Ma, J. F. (2010) Plasma membrane-localized transporter for aluminum in rice. *Proc. Natl. Acad. Sci. U.S.A.* **107,** 18381–18385 CrossRef Medline
39. Krishnamurthy, H., and Gouaux, E. (2012) X-ray structures of LeuT in substrate-free outward-open and apo inward-open states. *Nature* **481,** 469–474 CrossRef Medline
40. Kazmier, K., Sharma, S., Quick, M., Islam, S. M., Roux, B., Weinstein, H., Javitch, J. A., and McHaourab, H. S. (2014) Conformational dynamics of ligand-dependent alternating access in LeuT. *Nat. Struct. Mol. Biol.* **21,** 472–479 CrossRef Medline
41. Grouleff, J., Søndergaard, S., Koldsø, H., and Schiøtt, B. (2015) Properties of an inward-facing state of LeuT: conformational stability and substrate release. *Biophys. J.* **108,** 1390–1399 CrossRef Medline
42. Shaikh, S. A., and Tajkhorshid, E. (2010) Modeling and dynamics of the inward-facing state of a Na+/Cl−-dependent neurotransmitter transporter homologue. *PLoS Comput. Biol.* **6,** e1000905 CrossRef Medline
43. LeVine, M. V., and Weinstein, H. (2014) NbIT: a new information theory-based analysis of allosteric mechanisms reveals residues that underlie function in the leucine transporter LeuT. *PLoS Comput. Biol.* **10,** e1003603 CrossRef Medline
44. Forrest, L. R., Zhang, Y. W., Jacobs, M. T., Gesmonde, J., Xie, L., Honig, B. H., and Rudnick, G. (2008) Mechanism for alternating access in neurotransmitter transporters. *Proc. Natl. Acad. Sci. U.S.A.* **105,** 10338–10343 CrossRef Medline
45. Shan, J., Javitch, J. A., Shi, L., and Weinstein, H. (2011) The substrate-driven transition to an inward-facing conformation in the functional mechanism of the dopamine transporter. *PLoS ONE* **6,** e16350 CrossRef Medline
46. Zhao, Y., Quick, M., Shi, L., Mehler, E. L., Weinstein, H., and Javitch, J. A. (2010) Substrate-dependent proton antiport in neurotransmitter:sodium symporters. *Nat Chem Biol* **6,** 109–116 CrossRef Medline
47. LeVine, M. V., Terry, D. S., Khelashvili, G., Siegel, Z. S., Quick, M., Javitch, J. A., Blanchard, S. C., and Weinstein, H. (2019) The allosteric mechanism of substrate-specific transport in SLC6 is mediated by a volumetric sensor. *Proc. Natl. Acad. Sci. U.S.A.* **116,** 15947–15956 CrossRef Medline
48. Haemig, H. A., and Brooker, R. J. (2004) Importance of conserved acidic residues in mntH, the Nramp homolog of *Escherichia coli*. *J. Membr. Biol.* **201,** 97–107 CrossRef Medline
49. Chaloupka, R., Courville, P., Veyrier, F., Knudsen, B., Tompkins, T. A., and Cellier, M. F. (2005) Identification of functional amino acids in the Nramp family by a combination of evolutionary analysis and biophysical studies of metal and proton cotransport *in vivo*. *Biochemistry* **44,** 726–733 CrossRef Medline
50. Li, J., Wang, L., Zheng, L., Wang, Y., Chen, X., and Zhang, W. (2018) A functional study identifying critical residues involving metal transport activity and selectivity in natural resistance-associated macrophage protein 3 in *Arabidopsis thaliana*. *Int. J. Mol. Sci.* **19,** E1430 Medline
51. Bardou-Jacquet, E., Island, M. L., Jouanolle, A. M., Détivaud, L., Fatih, N., Ropert, M., Brissot, E., Mosser, A., Maisonneuve, H., Brissot, P., and Loréal, O. (2011) A novel N491S mutation in the human SLC11A2 gene impairs protein trafficking and in association with the G212V mutation leads to microcytic anemia and liver iron overload. *Blood Cells Mol. Dis.* **47,** 243–248 CrossRef Medline
52. Beaumont, C., Delaunay, J., Hetet, G., Grandchamp, B., de Montalembert, M., and Tchernia, G. (2006) Two new human DMT1 gene mutations in a patient with microcytic anemia, low ferritinemia, and liver iron overload. *Blood* **107,** 4168–4170 CrossRef Medline
53. Iolascon, A., d'Apolito, M., Servedio, V., Cimmino, F., Piga, A., and Camaschella, C. (2006) Microcytic anemia and hepatic iron overload in a child with compound heterozygous mutations in DMT1 (SCL11A2). *Blood* **107,** 349–354 CrossRef Medline
54. Lam-Yuk-Tseung, S., Camaschella, C., Iolascon, A., and Gros, P. (2006) A novel R416C mutation in human DMT1 (SLC11A2) displays pleiotropic effects on function and causes microcytic anemia and hepatic iron overload. *Blood Cells Mol. Dis.* **36,** 347–354 CrossRef Medline
55. Fleming, M. D., Romano, M. A., Su, M. A., Garrick, L. M., Garrick, M. D., and Andrews, N. C. (1998) Nramp2 is mutated in the anemic Belgrade (b) rat: evidence of a role for Nramp2 in endosomal iron transport. *Proc. Natl. Acad. Sci. U.S.A.* **95,** 1148–1153 CrossRef Medline
56. Lam-Yuk-Tseung, S., Mathieu, M., and Gros, P. (2005) Functional characterization of the E399D DMT1/NRAMP2/SLC11A2 protein produced by an exon 12 mutation in a patient with microcytic anemia and iron overload. *Blood Cells Mol. Dis.* **35,** 212–216 CrossRef Medline
57. Tavoulari, S., Margheritis, E., Nagarajan, A., DeWitt, D. C., Zhang, Y. W., Rosado, E., Ravera, S., Rhoades, E., Forrest, L. R., and Rudnick, G. (2016) Two Na^+ sites control conformational change in a neurotransmitter transporter homolog. *J. Biol. Chem.* **291,** 1456–1471 CrossRef Medline

58. Zhao, Y., Terry, D. S., Shi, L., Quick, M., Weinstein, H., Blanchard, S. C., and Javitch, J. A. (2011) Substrate-modulated gating dynamics in a Na^+-coupled neurotransmitter transporter homologue. *Nature* **474,** 109–113 CrossRef Medline
59. Chen, T. W., Wardill, T. J., Sun, Y., Pulver, S. R., Renninger, S. L., Baohan, A., Schreiter, E. R., Kerr, R. A., Orger, M. B., Jayaraman, V., Looger, L. L., Svoboda, K., and Kim, D. S. (2013) Ultrasensitive fluorescent proteins for imaging neuronal activity. *Nature* **499,** 295–300 CrossRef Medline
60. Senguen, F. T., and Grabarek, Z. (2012) X-ray structures of magnesium and manganese complexes with the N-terminal domain of calmodulin: insights into the mechanism and specificity of metal ion binding to an EF-hand. *Biochemistry* **51,** 6182–6194 CrossRef Medline